IAC-11.A7.2.1: GAMMA-RAY ASTRONOMY TECHNOLOGY NEEDS

N. Gehrels* and J. K. Cannizzo†

*Astroparticle Physics Laboratory, NASA/Goddard Space Flight Center, Greenbelt, MD 20771, USA
†Astroparticle Physics Laboratory, JCA/CRESST/UMBC, NASA/Goddard Space Flight Center, Greenbelt, MD 20771, USA

Abstract. In recent decades γ–ray observations have become a valuable tool for studying the universe. Progress made in diverse areas such as gamma-ray bursts (GRBs), nucleosynthesis, and active galactic nuclei (AGNs) has complimented and enriched our astrophysical understanding in many ways. We present an overview of current and future planned space γ–ray missions and discussion technology needs for the next generation of space γ–ray instruments.

Keywords: Gamma rays: general - telescopes - bursts - blazars - Galactic transients
PACS: 97.60.Bw, 98.70.Rz

1. BACKGROUND

The physics of photon interaction inside a medium as a function of energy divides naturally into three regimes: (1) photoelectric interactions at energies $E < 1$ mega-electron volts (MeV), (2) Compton scattering for $E \simeq 1$ MeV, and (3) pair production for $E \gtrsim 1$ MeV (Figure 1). This physical ordering by energy has given rise to three basic designs for high energy astronomical detectors: (i) coded aperture masks at low energies, where the illumination of an array grid casts a shadow on a detector, thereby providing information for an on-board computer to determine a position on the sky (e.g., the *Swift*/Burst Alert Telescope – BAT), (ii) a Compton telescope at medium energies (e.g., the *Compton Gamma-Ray Observatory*/Imaging Compton Telescope – *CGRO*/COMPTEL), and (iii) a pair telescope at high energies where an incident high-energy γ–ray interacts with the detector to produce a $e^- - e^+$ pair that is detected in a secondary phase. The detection strategy can be based on scintillators, solid state detectors, or pair trackers. Figure 2 indicates recent, current, and future high energy astrophysics missions.

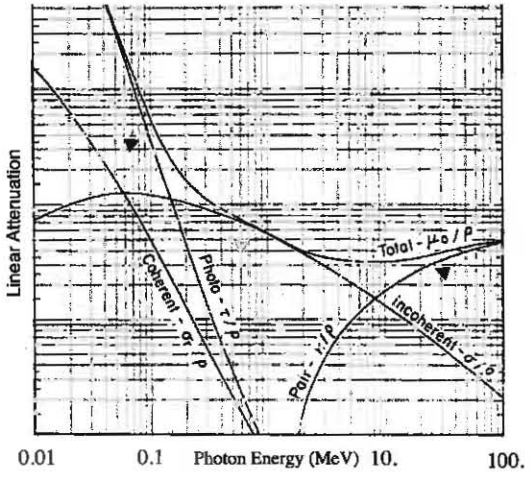

FIGURE 1. A schematic representation of photon interactions indicating linear attenuation in an absorptive medium versus energy. The small arrows indicate the dominant physical processes in each energy regime, photoelectric absorption and emission (red), Compton scattering (green) and pair production (blue).

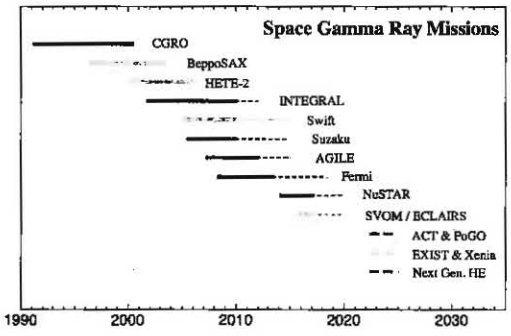

FIGURE 2. Space Gamma Ray Missions

2. GRBS

Of the missions indicated in Figure 2, those which have been the fundamental drivers in GRB research have been *CGRO*, the Italian-Dutch *Beppo Satellite for X-ray astronomy* (*BeppoSAX*), the *second High Energy Transient Explorer* (*HETE-2*), the *Swift Gamma-Ray Burst Mission* (*Swift*), and the *Fermi Gamma-ray Space Telescope* (*Fermi*). In *CGRO*'s mission length of >9 yr, the Burst and Transient Source Experiment (BATSE) provided localizations of several arcmin for $\sim$ 3000 GRBs, definitively establishing their isotropic distribution on the sky (Figure 3).

Science

During the *CGRO* era the lack of any apparent clustering along the galactic plane in the distribution of GRBs indicated a distance scale for GRBs either much smaller than galactic, or much larger. The latter case proved ultimately to be true, i.e., GRBs lie at cosmological distances. The first precise localizations came in 1997 from X-ray imaging by *BeppoSAX* with GRB 970228 and GRB 970508. These yielded host galaxies and subsequent redshifts. The first localization of a short GRB, including a probable host galaxy, came eight years later with *Swift* (GRB 050509B - Gehrels et al. 2005). A few months later *HETE-2* provided an even better short GRB localization, aided by an optical counterpart, that definitively identified the $z = 0.161$ host galaxy (GRB 050709 - Hjorth et al. 2005). *Swift* has now found over 500 GRBs, and the total number of GRBs with associated redshifts is well over 200 – the majority of these being *Swift* GRBs. The frequency histogram distribution of all redshift values z is a consistent tracer of the comoving volume of the Universe.

Figure 4 shows the isotropic distribution of GRBs as seen in *Fermi*/Gamma-ray Burst Monitor – GBM, which has detected over 700 to date. With its ability to study the temporal history of a GRB in detail over a broad range in energies, *Fermi* has placed strong constraints on possible violations of Lorentz invariance by the lack of time offsets between specific spikes in GRB light curves in different energy bands. For instance, in the short GRB 090510, for which $z = 0.903$, there was extended emission at both MeV and gigaelectron volt (GeV) energies, and also no observed dispersion in the inferred light travel time in going from kiloelectron volt (keV) to GeV energies (Figure 5, from Abdo et al. 2009).

Understanding of the GRB-supernova (SN) connection has advanced considerably as a result of *Swift*. An example of one such object is GRB 060218 which was a superlong GRB, with a duration of about 35 minutes. It was observed by the *Swift*/BAT, the X-ray telescope (XRT), and the ultraviolet-optical telescope (UVOT), and found through optical studies to lie at a redshift of $z = 0.033$. It was associated with SN 2006aj (Figure 6), an SN Ib/c with an isotropic energy equivalent of a few 10^{49} erg, thus underluminous compared to the overall energy distribution for long GRBs.

Technology

BATSE consisted of eight identical sodium iodide (NaI) Large Area Detector (LAD) modules, one at each of the satellite's corners, with sensitivity from 20 keV to 2 MeV. Each module measured 50.48 cm in diameter by 1.27 cm thick, with a 12.7 cm diameter 7.62 cm thick NaI spectroscopy detector, which extended the upper energy range to 8 MeV, all surrounded by a plastic scintillator in active anti-coincidence to veto the large background rates due to cosmic rays and trapped radiation.

The successor to *CGRO* in terms of making advances in GRB research has been *Swift*. The discovery instrument is the BAT hard X-ray transient monitor which has a large field of view (FoV) ($\sim$ 2 sr) and operates between about 15 and 150 keV. The detector consists of 256 modules of 128 individual cadmium zinc telluride (CZT) elements, each 4 mm by 4 mm by 2 mm, with a to-

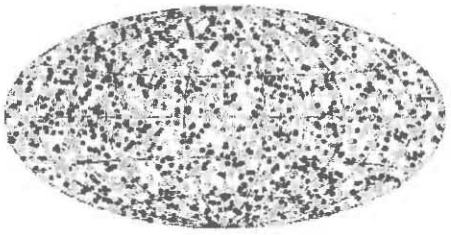

FIGURE 3. The isotropic distribution of 2704 GRBs found by *CGRO*/BATSE.

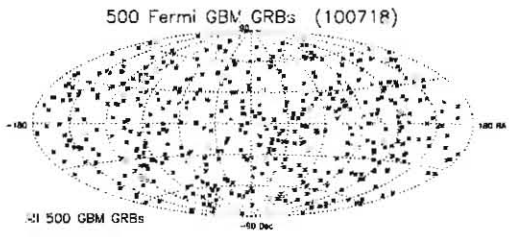

FIGURE 4. The isotropic distribution of GRBs found by *Fermi*/GBM.

tal detecting area of 5200 cm^2. Illumination of the coded aperture mask by the GRB casts a shadow in γ–rays on the BAT detector array, which allows an on-board computer to rapidly compute a $\sim 1-3$ arcmin localization which is broadcast to the astronomical community within $\sim 15-20$ s. A spacecraft slew is also initiated so that observations with the two narrow-field instruments, the UV telescope and the X-ray telescope, can commence within ~ 100 s.

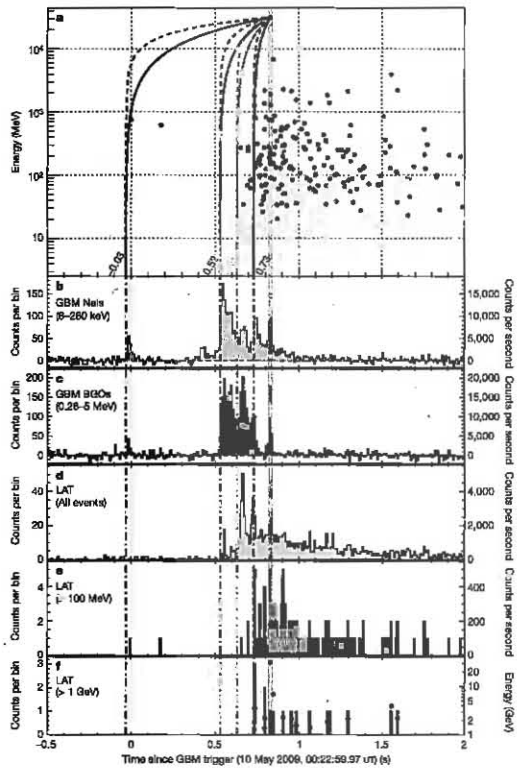

FIGURE 5. Light curves of GRB 090510 at different energies (Abdo et al. 2009).

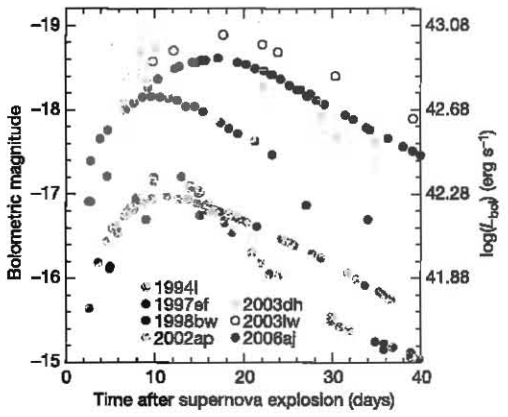

FIGURE 6. SN 2006aj, a SN Ic associated with GRB 060218 (Pian et al. 2006).

The *Fermi*/GBM includes twelve NaI scintillation detectors and two bismuth germanate (BGO) scintillation detectors. The NaI detectors cover the lower part of the energy range, from a few keV to ~1 MeV and provide burst triggers and locations. The BGO detectors cover ~150 keV to ~30 MeV, providing a good overlap with the NaI at the lower end, and with the LAT at the high end. Together the NaI and BGO detectors have similar characteristics to the combination of the BATSE large area and spectroscopy detectors but cover a wider energy range and have a smaller collection area. The detectors do not block any part of the Large Area Telescope (LAT) FoV. They fit between the LAT and the shroud envelope on two sides of the spacecraft. The mounting arrangement is flexible with the two BGO detectors mounted on opposite sides of the spacecraft, and the NaI detectors mounted in 4 banks of 3 detectors so that they sample a wide range of azimuth and elevation angles.

The *Fermi* LAT detects individual γ–rays after they strike the detector and produce $e^- - e^+$ pairs. These charged particles pass through interleaved layers of Si microstrip detectors, inducing a current. The incident path is reconstructed using information from several layers of tracker layers. After passing through the tracker, the particles enter the calorimeter, which consists of a stack of cesium iodide (CsI) scintillator crystals to measure the total energy of the particles. The LAT FoV is ~2.5 sr. The image resolution varies from a few arcmin the highest-energy photons to ~3° at 100 MeV. The LAT is a larger, improved version of the *CGRO* Energetic Gamma Ray Experiment Telescope (EGRET).

The *Energetic X-ray Imaging Survey Telescope* (*EXIST*) and *Xenia* (the Greek word for "hospitality") are two future mission concepts which will optimize future studies of the GRB/SN connection:

The High Energy Telescope (HET) is the primary instrument on *EXIST*, which will consist of 4.5 m^2 of imaging CZT detectors in a wide-field coded aperture telescope. It covers the $5-600$ keV band and images sources in a $\sim 70° \times 90°$ FoV, with 2 arcmin resolution and $\lesssim 20$ arcsec positions (90% confidence radius) for $\gtrsim 5\sigma$ survey threshold detections.

On *Xenia*, the Transient Event Detector (TED) will monitor a ~ 3 sr solid angle and will localize GRBs with a fluence greater than 10^{-6} erg cm^{-2} ($15-150$ keV), with a positional uncertainty < 4 arcmin. It will locate a sufficient number (> 50 yr^{-1}) of GRBs with after-

TABLE 1. Future GRB Technology Needs

• Hard X-ray detectors for wide-field transient detection
• high stopping power (high density and atomic number)
• pixellated (mm resolution)
• room temperature operation
• medium-to-high spectral resolution (~percent)
• CZT detectors under development
• Large number of pixels
• High resolution X-ray spectroscopy needed for *Xenia* WIM
• Rapidly slewing, autonomous spacecraft
• Rapid downlink capability

glows bright enough for the other *Xenia* instruments to determine the absorption from the warm hot intergalactic medium (WHIM) and to measure the cosmic history of metals at GRB sites. TED will have sensitivity in the $8-200$ keV range. TED is a coded mask instrument based on CZT detector technology. The design has two identical coded mask telescopes, tilted by 28° with respect to the optical axis of the two *Xenia* narrow field instruments High Angular Resolution Imager (HARI) and Cryogenic Imaging Spectrometer (CRIS). This results in a sky coverage as large as 2.8 sr. For bursts with fluence exceeding 2×10^{-6} erg cm^{-2}, the FoV is increased to 3.9 sr. The sensitivity of TED is similar to the *Swift*/BAT instrument and sufficient to detect and localize about 80 bursts with a prompt fluence greater than 10^{-6} erg cm^{-2} yr^{-1}. With a distance to the mask of 40.5 cm and a pixel size of 2.7 mm, a location accuracy < 4 arcmin is achieved for sources with a signal-to-noise ratio greater than 10. This is sufficient to trigger fast repointing and to position the source in the 6 arcmin by 6 arcmin FoV of the high count rate section of the CRIS.

Table 1 indicates the future technology needs for GRB research.

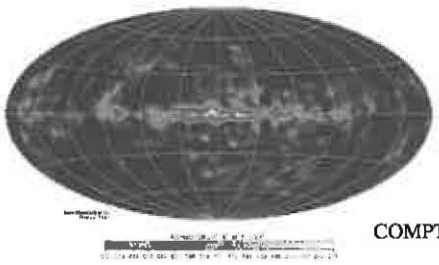

FIGURE 7. A galactic intensity distribution map of the ^{26}Al 1809 keV line as measured by *CGRO*/COMPTEL.

3. NUCLEOSYNTHESIS

The two primary workhorses to date in this endeavor have been *CGRO*/COMPTEL and the *INTEGRAL* Spectrometer (SPI). Figure 7 shows the galactic map of ^{26}Al 1809 keV line emission from COMPTEL, and Figure 8 shows a measurement of the Doppler-shift in the ^{26}Al 1809 keV line profile as a function of galactic longitude.

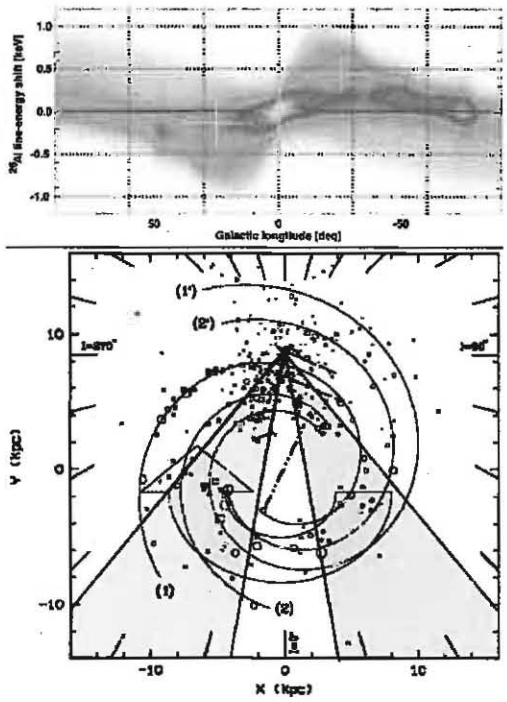

FIGURE 8. A comparison of the Doppler-shift signature from ^{26}Al sources, as observed with *INTEGRAL*/SPI (Diehl et al. 2006).

TABLE 2. Future Nucleosynthesis Technology Needs

• Detectors for γ–ray spectroscopy and imaging
• high stopping power (high density and atomic number)
• pixellated (mm resolution)
• high spectral resolution (~percent)
• Ge strip detectors under development
• Large number of pixels
• Layers of Si and CZT detectors also possible
• Large number of pixels

Science

The study of the ^{26}Al 1809 keV line in the galaxy has provided a window on galactic structure (Diehl et al. 2006) completely orthogonal to the traditional studies based on the 21 cm spin-flip transition in atomic hydrogen, and from IR studies of intragalactic medium.

Technology

The COMPTEL instrument (Schönfelder 1991) on *CGRO* combined a large FoV with imaging. It consisted of two detector arrays, and upper one of low-Z material and a lower one of high-Z material. In the upper detector an incoming γ–ray was Compton scattered, and the scattered photon subsequently made a second interaction in the lower detector. A time-of-flight measurement was utilized to confirm the causal relation. The locations and energy losses of both interactions were monitored. For events that were completely absorbed, the arrival direction of the γ–ray had to lie within a known angle of the direction of the scattered γ–ray, which allowed a determination of its original direction on the sky. Incompletely absorbed events yielded uncertainty cones that did not constrain the source position.

The SPI (SPectrometer on *INTEGRAL*) does spectral analysis of γ–ray point sources and extended regions in the 20 keV - 8 MeV energy range with an energy resolution $\Delta E \simeq 2$ keV full-width at half maximum (FWHM) at 1 MeV. This is done using an array of 19 hexagonal high purity Ge detectors cooled to 85 K. A hexagonal coded aperture mask is located 1.7 m above the detection plane in order to image large regions of the sky (16° fully coded FoV) with an angular resolution of 2°. To reduce background radiation the detector assembly is shielded by a veto (anticoincidence) system which extends around the bottom and side of the detector almost completely up to the coded mask. The aperture (and hence contribution by cosmic diffuse radiation) is limited to $\sim 30°$. A plastic veto is provided below the mask to further reduce the 511 keV background.

The Advanced Compton Telescope (ACT) is currently in the mission concept phase. Technology development is still required in order to make it possible. It will have a medium energy range of $0.2 - 10$ MeV and be able to study nuclear γ–ray lines in pulsars and blazars. Figure 9 shows a simulation from the ACT Study Report (Boggs et al. 2006) indicating the expected data quality from a SN at 10 Mpc. The modeled nuclear decay line is a tracer for ^{56}Ni $\rightarrow^{56}$ Co $\rightarrow^{56}$ Fe. For comparison, Figure 10 shows an observation of the same nuclear transition line seen in SN1987A at 50 kpc by the balloon experiment Gamma-Ray Imaging Spectrometer (GRIS).

With Compton imaging, an incoming γ–ray photon Compton scatters off an electron, and the recoiling electron induces a signal in the detector. The scattered photon then undergoes one or more interactions, which are

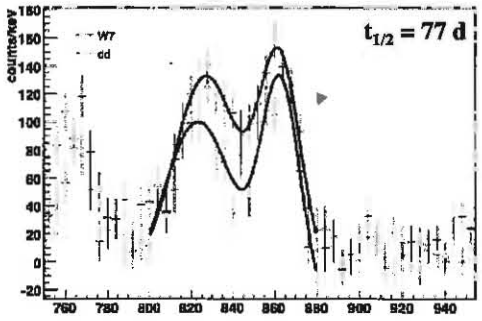

FIGURE 9. A simulation of an observation by ACT of a SN at 10 Mpc.

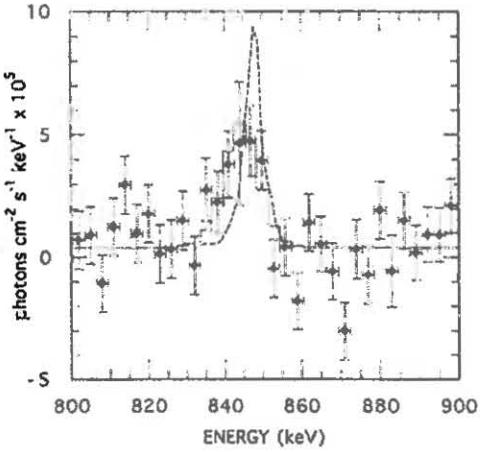

FIGURE 10. GRIS data of the 847 keV ^{56}Co decay line in SN 1987A at 613 d after the SN (Tueller et al. 1990).

TABLE 3. ACT Science Requirements

Energy Range	$0.2-30$ MeV Compton mode
Energy Resolution	< 10 keV FWHM @ 1 MeV
Field of View	> 4 sr
Angular Resolution	1 deg
Source Localization	5 arcmin for bright sources
Line Sensitivity	10^{-7} ph cm^{-2} s^{-1} (narrow)
in 10^6 s	5×10^{-7} ph cm^{-2} s^{-1} (broad)
Continuum Sensitivity	10^{-5} ph cm^{-2} s^{-1} MeV^{-1} @ 0.5 MeV
Polarization Sensitivity	1%, 2×10^{-3} ph cm^{-2} s^{-1} MeV^{-1}
	10%, 2×10^{-4} ph cm^{-2} s^{-1} MeV^{-1}

also recorded. The total energy of the incoming photon and its initial incident direction can be reconstructed. The sky position can be constrained along a circle or arc on the sky, depending on the instrument's capability to record recoil electron tracks. Two instrumental uncertainties contribute to the finite width of the event circle: the uncertainty due to the finite energy resolution, and the uncertainty due to the finite spatial resolution. There is also a fundamental limit on the width of the event circle set by Doppler broadening due to Compton scattering on bound electrons.

Table 2 indicates the future technology needs for nucleosynthesis research.

4. AGNS

AGNs are thought to be accretion powered supermassive black holes (SMBHs). Their bolometric luminosities can be as high as $\sim 10^{45}$ erg s^{-1}. The high energy missions which have had the most impact to date on AGN research are *CGRO*/EGRET, *Swift*/BAT, and *Suzaku*/Hard X-ray Detector (HXD). Broadband spectra for the two main classes of γ–ray AGN are shown in Figure 11. The Seyferts show emission up to ~ 1 MeV, whereas the blazars can have emission out to $\gtrsim 10^6$ MeV.

Science

Blazars represent one type of AGN. They are very compact quasars associated with a SMBH at the center of an active, giant elliptical galaxy. We observe "down" a relativistic jet that is pointing in the general direction of the Earth, or nearly so, and this accounts for the rapid variability and compact features of both types of blazars. Many blazars have apparent superluminal features within the first few parsecs of their jets. The study of blazars was catapulted into a major field of study by the wealth of systems found by *CGRO*/EGRET (Fichtel et al. 1994). Figure 12 shows an EGRET view of the blazar 3C 279.

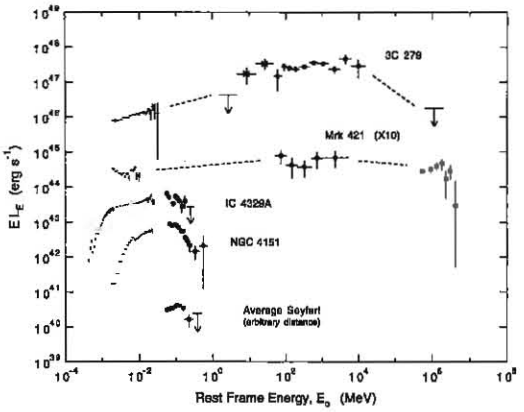

FIGURE 11. A comparison of blazars (3C 279, Mrk 421) with Seyferts (IC 4329A, NGC 4151). Shown is the luminosity per natural logarithmic energy interval $EL_E = 4\pi d_L^2 E^2 \Phi(E)$, as a function of rest-frame energy $E_0 = (1+z)E$, where $\Phi(E)$ is the photon flux in cm^{-2} s^{-1} MeV^{-1} and d_L is the luminosity distance. From Dermer & Gehrels (1995).

FIGURE 12. A view of the blazar 3C 279 by *CGRO*/EGRET (Hartman et al. 1992).

Figure 13 presents a significant inverse correlation between γ–ray spectral index and X-ray spectral index found in a *Fermi* sample of bright blazars (Abdo et al. 2010b).

AGN surveys based on high energy observations do not suffer from the same biasing select effects stemming from absorption at low energies that afflict lower energy surveys. (Figure 14 shows an example of a low energy observation in X-rays of a heavily absorbed Seyfert 2.) For instance, the *Swift*/BAT survey of AGN (Tueller et al. 2008) is already revealing interesting differences in demographics from prior surveys based on $2-10$ keV X-rays. Figure 15 shows a result from the first *Fermi* AGN catalog – the photon spectral index as a function of γ–ray luminosity L_γ, spanning ten decades in L_γ (Abdo et al. 2010a).

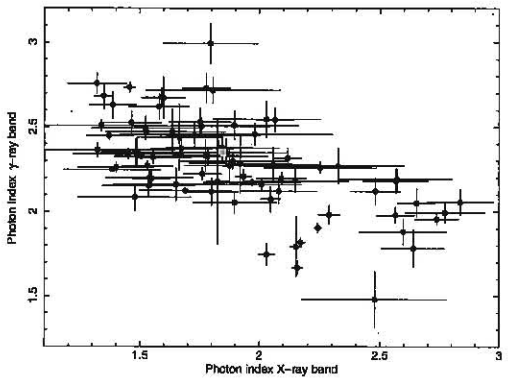

FIGURE 13. From a study of the *Fermi* bright blazars (Abdo et al. 2010b), the γ–ray band power law spectral index plotted against the X-ray spectral index. One sees a correlation, as expected in synchrotron-inverse Compton scenarios (Padovani & Giommi 1996).

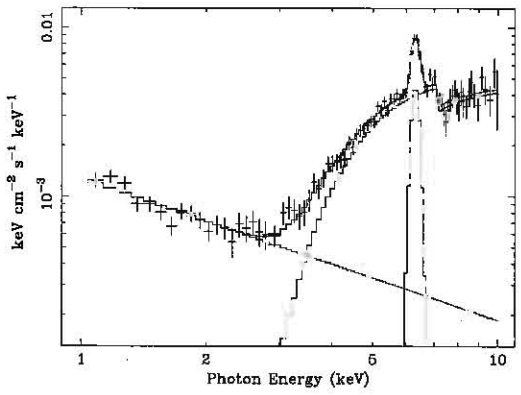

FIGURE 14. An observation of an absorbed Seyfert 2 (Moran et al. 2001).

Technology

CGRO/EGRET had energy coverage from 20 MeV to about 30 GeV. It used a multilevel thin-plate spark chamber system to detect γ–rays by the $e^- - e^+$ pair production process. A calorimeter using NaI(Tl) under the instrument provided good energy resolution over a wide dynamic range. The instrument was covered by a plastic scintillator anticoincidence dome to prevent triggering on events not associated with γ–rays. The combination of high energies and good spatial resolution in EGRET provided the best source positions of any *CGRO* instrument. A γ–ray entering EGRET within the acceptance angle had a reasonable probability (about 35% above 200 MeV) of converting into an $e^- - e^+$ pair in one of the thin plates between the spark chambers in the upper portion of the telescope. If at least one particle of the pair was detected by the directional time-of-flight coincidence system as a downward moving particle, and if there were no signal in the large anticoincidence scintillator surrounding the upper portion of the telescope, the track imaging system was triggered, providing a digital picture of the γ–ray event, and the analysis of the energy signal from the NaI(Tl) detector was initiated. Incident charged particles were rejected by the anticoincidence dome.

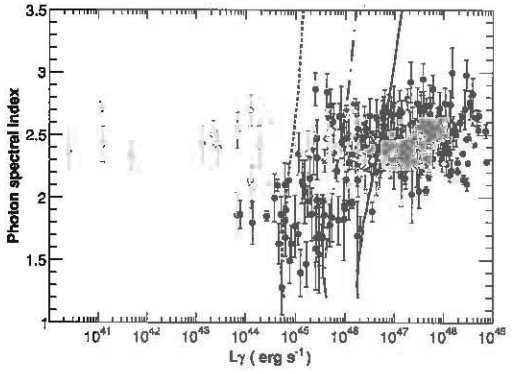

FIGURE 15. From the first *Fermi* AGN catalog (Abdo et al. 2010a), the photon spectral index versus γ–ray luminosity for different AGN classes (red: flat-spectrum radio quasars (FSRQs); green: low-synchrotron-peaked BL Lacertae (LSP-BL Lac); cyan: intermediate-synchrotron-peaked BL Lacs (ISP-BL Lac); blue: high-synchrotron-peaked BL Lacs (HSP-BL Lac); magneta: radio galaxies). The curves indicate approximate instrumental limits for $z = 0.2$ (dashed), $z = 0.5$ (dot-dashed), and $z = 1$ (solid).

The *Suzaku*/HXD covers $10-700$ keV using a combination of GSO well-type phoswich counters (> 50 keV) and the Si PIN diodes (< 50 keV). The HXD has a low background; its sensitivity is higher than any past missions in the hard X-ray band. The HXD consists of 16 identical detector units in a 4 by 4 arrangement. The four sides of the detector units are surrounded by 20 thick anti-counters made of BGO. The anti-counters also detect GRBs, determined their sky positions from the ratios of the numbers of events detected by different anti-counters. Each detector unit is furthermore divided into four deep wells by the BGO active shields. Although the detector does not have imaging capability, the FoV is limited by the shielded well. At the bottom of each well lies a GSO crystal into which photons with $E \gtrsim 50$ keV are deposited. These events, which are detected by the GSO but not by the surrounding BGO, are deemed "clean hit" events (i.e., astrophysical).

Scheduled for launch in 2012, the Nuclear Spectroscopic Telescope Array (NuSTAR) is a hard X-ray focusing mission with $\sim$100 times better sensitivity than coded masks. It will undertake an AGN survey, imaging of SN remnants, and coordinated GeV/teraelectron volt (TeV) observations with ground based Cerenkov air shower observatories.

The NuSTAR instrument consists of two co-aligned grazing incidence telescopes with specially coated optics and newly developed detectors that extend sensitivity to higher energies as compared to previous missions such as the *Chandra X-ray Observatory* (*Chandra*) and the *X-ray Multi-Mirror Mission* (*XMM*). After launching into orbit on a small rocket, the NuSTAR telescope extends to achieve a 10 m focal length. The observatory will provide a combination of sensitivity, spatial, and spectral resolution factors of 10 to 100 improved over previous missions that have operated at these X-ray energies. Figure 16 shows a comparison of the sensivity of NuSTAR with other hard X-ray instruments.

NuSTAR has two detector units, each at the focus of one of the two co-aligned NuSTAR optics units. The optical units observe the same area of sky, and the two images are combined on the ground. The focal planes are each comprised of four 32×32 pixel CZT detectors. The electrons are then digitally recorded using custom Application Specific Integrated Circuits (ASICs) designed by the NuSTAR Caltech Focal Plane Team.

The focal planes are shielded by CsI crystals surrounding the detector housings. The crystal shields register high energy photons and cosmic rays crossing the focal plane from directions other than the along the optical axis. Such events are the primary background and must be properly identified and subtracted in order to identify high energy photons from cosmic sources. The active shielding ensures that any CZT detector event coincident with an active shield event is ignored.

For high energy γ–rays, future technologies include scintillating fibers, Ge strip detectors, and three dimensional (3D) gas micropattern detectors. Figure 17 shows a comparison of the sensitivities of current and future observatories. The five year capability of *Fermi* at energies of $\sim 1-10$ GeV compares favorably with an extrapolation to lower energies of 50 hr integrations from the Cerenkov shower observatories, the Very Energetic Radiation Imaging Telescope Array System (VERITAS) and the F. L. Whipple Observatory (Whipple). Upcoming studies should enable detailed broad-band studies of nature's accelerators, in particular jet outflows, shock acceleration, and magnetic reconnection.

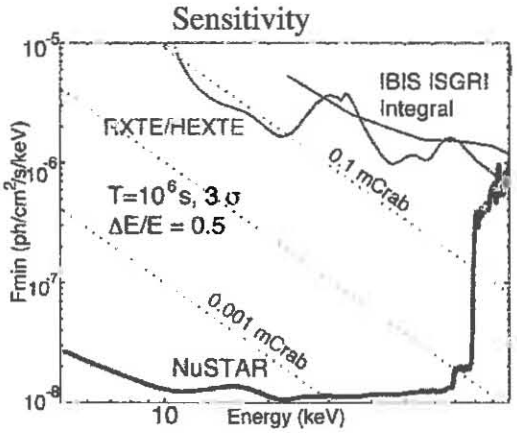

FIGURE 16. A comparison of the sensivity of NuSTAR with other hard X-ray instruments.

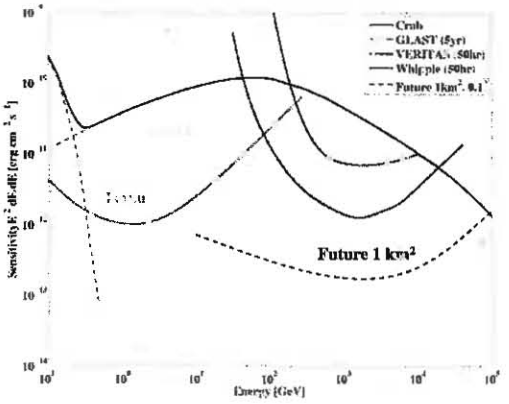

FIGURE 17. A comparison of sensitivities of current and future observatories.

TABLE 4. Future AGN Technology Needs

• Detectors for high energy γ–rays
• Mirrors for focusing hard X-ray photons
• Grazing incidence mirrors
• Multilayer Bragg technique for hard X-ray response
• Lens for concentrating γ–ray photons
• Laue lenses
• Fresnel lenses
• Detectors for hard X-ray polarization measurement
• Multi-element, multi-technology for Compton detection

Table 4 indicates the future technology needs for AGN research.

5. CONCLUSION

The future is bright for γ–ray astronomy. Instruments in development are pushing the technology frontier in areas of focusing telescopes, polarization and wide-field imaging. Beyond the current missions, new technologies are being developed that will greatly expand capabilities for high sensitivity, high angular resolution and high spectral resolution.

REFERENCES

1. A. A. Abdo, et al., *Nature*, 2009, 462, 331.
2. A. A. Abdo, et al., *ApJ*, 2010a, 715, 429.
3. A. A. Abdo, et al., *ApJ*, 2010b, 716, 30.
4. S. E. Boggs, et al., *arXiv:astro-ph/0608532v1*, 2006.
5. C. D. Dermer, and N. Gehrels, *ApJ*, 1995, 447, 103.
6. R. Diehl, et al., Proc. 6th *INTEGRAL* Workshop "The Obscured Universe", Moscow, 3-7 July 2006.
7. C. E. Fichtel, et al., *ApJ*, 1994, 94, 551.
8. N. Gehrels, et al., *Nature*, 2005, 437, 851.
9. R. C. Hartman, et al., *ApJ*, 1992, 385, L1.
10. J. Hjorth, et al., *Nature*, 2005, 437, 859.
11. E. C. Moran, L. E. Kay, M. Davis, A. V. Filippenko, and A. J. Barth, *ApJ*, 2001, 556, L75.
12. P. Padovani, and P. Giommi, *MNRAS*, 1996, 279, 526.
13. E. Pian, et al., *Nature*, 2006, 442, 1011.
14. V. Schönfelder, *Advances in Space Research*, 1991, 11, 313.
15. J. Tueller, S. Barthelmy, N. Gehrels, B. J. Teegarden, M. Leventhal, and C. J. MacCallum, *ApJ*, 1990, 351, L41.
16. J. Tueller, et al., *ApJ*, 2008, 681, 113.